

Influence of the conductivity on spin wave propagation in a Permalloy waveguide

Cite as: J. Appl. Phys. **126**, 043904 (2019); <https://doi.org/10.1063/1.5110202>

Submitted: 15 May 2019 . Accepted: 06 July 2019 . Published Online: 23 July 2019

Takashi Manago, Mustafa M. Aziz, Feodor Ogrin, and Kenji Kasahara



View Online



Export Citation



CrossMark

Journal of
Applied Physics

SPECIAL TOPIC:
Polymer-Grafted Nanoparticles

Submit Today!

AIP
Publishing

Influence of the conductivity on spin wave propagation in a Permalloy waveguide

Cite as: J. Appl. Phys. 126, 043904 (2019); doi: 10.1063/1.5110202

Submitted: 15 May 2019 · Accepted: 6 July 2019 ·

Published Online: 23 July 2019



View Online



Export Citation



CrossMark

Takashi Manago,^{1,2,a)} Mustafa M. Aziz,³ Feodor Ogrin,² and Kenji Kasahara¹

AFFILIATIONS

¹Department of Applied Physics, Fukuoka University, Fukuoka 814-0180, Japan

²Department of Physics and Astronomy, University of Exeter, Exeter EX4 4QL, United Kingdom

³College of Engineering, Mathematics and Physical Sciences, University of Exeter, Exeter EX4 4QF, United Kingdom

^{a)}E-mail: manago@fukuoka-u.ac.jp

ABSTRACT

The influence of the electrical conductivity of a Permalloy waveguide on the spin wave propagation was investigated using the finite-element solution of the combined system of quasistatic electromagnetic potential and linearized LLG (Landau–Lifshitz–Gilbert) equations. The difference in the group velocity between the conductive and nonconductive waveguides becomes large for films over 300 nm thick, and the difference is very small for film thicknesses less than 100 nm. The observed enhancement of the group velocity with increasing film thickness is attributed to the damping caused by the electrical conductivity, which leads to narrowing of the spin wave packet envelope and shorter arrival times of propagating waves. The basic characteristics of the dispersion relations do not change between conductive and nonconductive films for small film thicknesses less than 300 nm. The simulated dispersion relations indicate shift of their maximum intensity toward lower wavenumbers and, therefore, increase in the group velocity with increasing thickness. The simulated decay length of the spin waves for conductive films initially increases but then decreases with increasing thickness, which agrees well with the experimental results. The extracted damping coefficients from both simulations and the experiment agree very well and increase proportionally with d^2 , where d is the film thickness, due to the additional eddy current damping. The observed thickness and conductivity dependence of spin wave propagation is crucial for magnonics research and toward the development of future spin wave devices using metal films.

Published under license by AIP Publishing. <https://doi.org/10.1063/1.5110202>

I. INTRODUCTION

Magnonics is one of the most fascinating research fields in spintronics. Spin waves, the collective precessional motion of the local magnetic moments, have been intensively investigated in studies of their fundamental properties and their applications in information transport and processing.^{1–12} An important perceived advantage of using spin waves is the low power consumption for information transport, as there are no moving charges, which avoids Joule heating. Additionally, their wave propagation properties allow functionalities such as logic gate operations. In order to integrate spin wave devices with conventional Si devices, ferromagnetic metals are favorable for waveguide materials rather than Yttrium Iron Garnets (YIGs) because of their Si process compatibility. Therefore, there is significant research interest in spin waves using metal waveguides such as Permalloy (Py) in information transport and processing applications. Examples include the first study of spin wave propagation spectroscopy in Py,¹³ time-resolved

measurement of spin wave propagation,¹⁴ Doppler shift of spin waves,^{15–17} studies of their basic properties of excitation and propagation,¹⁸ spin wave interference,¹⁹ the method of estimating the damping factor from spin waves,²⁰ and nonreciprocity of magneto-static surface waves (MSSW) in Py waveguides.^{21,22} In these reports, the thickness of the Py waveguide was few tens of nanometers and thinner than the skin depth (typically less than 100 nm),²³ where the effect of the electrical conductivity on spin wave propagation is negligible. Therefore, the reported results on these thin film waveguides and their analysis were consistent with the conventional theory of spin waves, which was formulated for magnetic insulators such as YIG.

In our previous paper on MSSW in Py, however, thicker waveguides showed a higher measured group velocity for the spin waves, but without a significant increase in their decay length.²⁴ Figure 1(a) shows typical measured magnetization waveforms for Py films of various thicknesses measured using a detection antenna

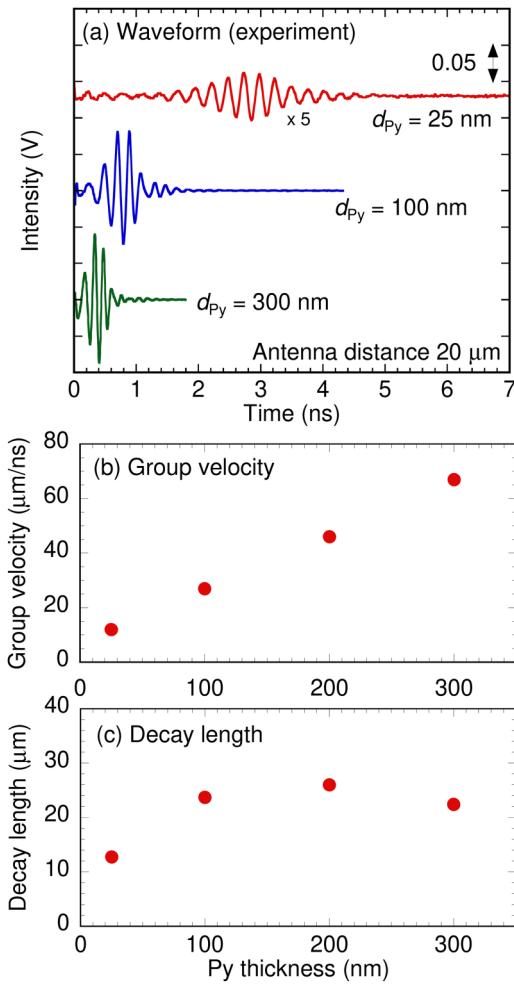


FIG. 1. (a) Typical measured magnetization waveforms for Py films of various thicknesses detected at 20 μm away from the edge of the excitation antenna. (b) Py thickness dependence of the measured group velocity. (c) Py thickness dependence of the measured decay length.

20 μm away from the excitation antenna. Shorter arrival time is observed for the thicker films, and the group velocity increases with Py thickness, as shown in Fig. 1(b). On the other hand, the decay length seems to saturate and then decrease with increasing Py thickness, as shown in Fig. 1(c). This is counterintuitive because the decay length should increase in proportion to the group velocity if the magnetic damping mechanism does not change. One of the candidates for the additional damping is the influence of the electrical conductivity of the waveguide. If the waveguide material were YIG, it is not necessary to take this additional damping into account because YIG is an insulator. However, Py is a metal, and so the finite conductivity could affect the spin wave propagation.

Precession of the magnetization in the Py layer induces eddy currents that could cause damping of the spin waves. Ament and Rado showed that eddy currents cause a finite ferromagnetic

resonance (FMR) linewidth even in the absence of damping.²⁵ Almeida and Mills presented the theory of eddy current damping and frequency renormalization of spin waves in conducting ferromagnetic films.²⁶ Maksymov and Kostylev showed that even though the energy dissipation by eddy currents leads to broadening of the linewidth, the increase in the in-plane magnetic field due to eddy currents is the principal mechanism responsible for the deviation from the dispersion relation of surface spin waves.²⁷ However, there is still lack of understanding about spin wave propagation in thick metal films and its damping characteristics. It is important to understand the spin dynamics in a wide range of film thicknesses systematically for designing and utilizing metal-based spin wave devices. In order to investigate the effects of the electrical conductivity on the group velocity and decay length, we performed combined electromagnetic-micromagnetic simulations incorporating the electrical conductivity of the magnetic film and compared the results with our previous experimental measurements on Py waveguides.²⁴

II. SIMULATION PROCEDURES

Simulations of the spin wave propagation incorporating conductivity were performed using the finite-element method (FEM) in COMSOL Multiphysics. In the FEM model, the quasistatic magnetic fields due to electric currents and magnetization sources are evaluated using the vector magnetic potential A ,

$$\sigma \frac{\partial A}{\partial t} + \nabla \times (\nabla \times A / \mu_0 - M) = J^e, \quad (1)$$

where σ is the electrical conductivity, J^e is the externally applied current density (in the excitation antenna), and M is the magnetization (zero outside the Py film). Time varying magnetic fields in the Py film (due to magnetization and external sources) will induce the currents $J^i = \sigma \partial A / \partial t$ in Eq. (1). A schematic cross section of the modeled Py strip and excitation antenna configuration is shown in Fig. 2. This is based on our experimental setup and sample

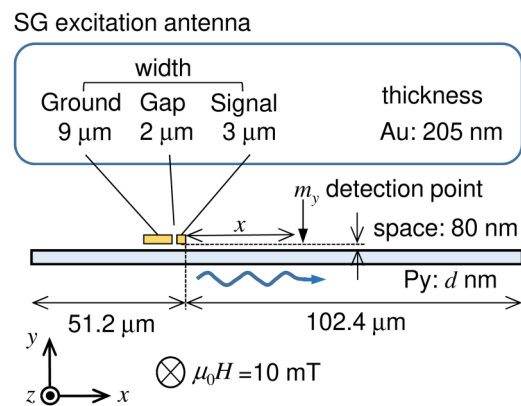


FIG. 2. Schematic cross section of the modeled Permalloy strip and excitation antenna configuration for the FEM simulation.

dimensions described in Ref. 24, where the width of the structure in the z -direction (Py film and antenna) is much larger than the other dimensions in the system. This permits the simplification of Eq. (1) to two dimensions and writing the vector potential $\mathbf{A} = A_z \mathbf{z}$ and $\mathbf{J}^a = J_z^a \mathbf{z}$, where \mathbf{z} is a unit vector in the z -direction, orthogonal to the magnetic fields $\mathbf{B} = \nabla \times \mathbf{A}$ in the x - and y -directions.

The magnetization \mathbf{M} in the Py film in Eq. (1) can be evaluated using the LLG (Landau–Lifshitz–Gilbert) equation,²⁸

$$\frac{d\mathbf{M}}{dt} = -\gamma(\mathbf{M} \times \mathbf{H}^{\text{eff}}) + \frac{\alpha}{M_S} \left(\mathbf{M} \times \frac{d\mathbf{M}}{dt} \right), \quad (2)$$

where \mathbf{H}^{eff} is the effective field, M_S is the saturation magnetization, α is the damping coefficient, γ is the gyromagnetic ratio, and t is the time. In the experimental arrangement in Ref. 24, a sufficiently strong saturating field H_z is applied across the Py film in the z -direction as indicated in Fig. 2. This leads to small perturbations in the dynamic magnetization in the neighborhood of the saturated state. In this case, we can write the magnetization and effective field as

$$\mathbf{M} = \begin{pmatrix} m_x \\ m_y \\ M_S + m_z \end{pmatrix}, \quad \mathbf{H} = \begin{pmatrix} h_x^{\text{eff}} \\ h_y^{\text{eff}} \\ H_z \end{pmatrix}. \quad (3)$$

Substituting Eq. (3) in the LLG equation in Eq. (2), solving for the time derivatives in magnetization and ignoring second and higher order terms (including α^2 and $m \cdot h$ terms), yields the linearized LLG equations used in the model,

$$\begin{aligned} \frac{dm_x}{dt} &\approx \gamma[\alpha(h_x^{\text{eff}} M_S - H_z m_x) + s(h_y^{\text{eff}} M_S - H_z m_y)], \\ \frac{dm_y}{dt} &\approx \gamma[\alpha(h_y^{\text{eff}} M_S - H_z m_y) - s(h_x^{\text{eff}} M_S - H_z m_x)], \\ \frac{dm_z}{dt} &\approx 0, \end{aligned} \quad (4)$$

where $s = \text{Signum}(H_z)$ to account for reversal in the direction of the applied bias field H_z . The effective field in Eq. (4) includes nearest neighbor exchange interactions and is given by

$$\begin{aligned} h_x^{\text{eff}} &= h_x + C\nabla^2 m_x, \\ h_y^{\text{eff}} &= h_y + C\nabla^2 m_y, \end{aligned} \quad (5)$$

where $C = 2A/\mu_0 M_S^2$, A is the exchange stiffness constant, and h_x and h_y include the contributions of the demagnetizing fields, anisotropy fields, applied antenna fields, and induced eddy current fields. The exchange boundary condition with no surface anisotropy, $\partial \mathbf{m} / \partial \mathbf{n} = 0$, was used to terminate the boundaries of the Py structure, where \mathbf{n} is the vector normal to the surface.

In the FEM model, the Py strip is $153.6 \mu\text{m}$ long and d nm thick ($d = 25\text{--}1000$ nm). The SG (Signal-Ground) type coplanar waveguide (CPW) consists of two Au conducting tracks. The

widths of the SG type antenna are $3 \mu\text{m}$ for the signal line, $2 \mu\text{m}$ for the gap, and $9 \mu\text{m}$ for the ground line, and their thickness is 205 nm. The currents in the two wires are equal in value but opposite in sign. The antenna is located at 80 nm above the Py surface, which corresponds to the thickness of the SiO_2 insulation layer of the actual sample. The Py material parameters used in the simulation are $M_S = 830$ kA/m, $\gamma = 2.337 \times 10^5$ m/(A s), $\alpha = 0.01$, and $A = 1.3 \times 10^{11}$ J/m. The uniform in-plane bias magnetic field in the Py strip is 10 mT along the z -direction. The electrical conductivities of the Py strip and Au antenna are $\sigma_{\text{Py}} = 5 \times 10^6$ S/m²⁹ and $\sigma_{\text{Au}} = 4 \times 10^7$ S/m, respectively, at room temperature. The calculations for $\sigma_{\text{Py}} = 0$ S/m were also performed for comparison. A Gaussian pulse excitation for J_z^e with a pulse amplitude corresponding to a 4 mA excitation current and a width of 50 ps was applied in the SG type antenna. We only used the out-of-plane component (y -component) of the simulated dynamic magnetization in the Py film for the spin wave propagation analysis, which is responsible for the surface poles and corresponding stray fields practically measured using a receiving antenna. The simulation space surrounding the waveguide structure in Fig. 2 is air with magnetically insulating boundaries sufficiently far from the waveguide structure to have negligible effects on the simulations while providing practical computation times. Adaptive meshing using triangular elements is used to sample the different dimensions of the waveguide structure, with a maximum element size of 50 nm in the Py layer. The dispersion of the MSSWs in the relevant wavelength range is dominated by the magneto-dipole interaction. Hence, our maximum element size is sufficient for an adequate description of the MSSWs. In a separate simulation, we verified that the use of smaller cells does not modify the results significantly. The maximum time step used in the simulations is 10 ps.

The fundamental wavenumber k_x of the excited spin wave in this antenna configuration is $0.34 \mu\text{m}^{-1}$, which is determined by the distance between the signal and ground lines of the antenna.³⁰ Actual excited spin waves, however, include a wide range of wave vectors in addition to the fundamental wavenumber and so become dispersive. Therefore, the actual waveforms of the wave packet may not be completely described by a Gaussian envelope. Nevertheless, Gaussian fitting has been widely used and practically beneficial for the experimental analysis of wave packet amplitude or peak measurements.²⁴ We used Gaussian fitting for our simulated results in order to perform the same analysis and to be consistent with the experimental results in Ref. 24. The arrival time and amplitude of the spin waves were extracted from the Gaussian fitting and enabled the estimation of the group velocity v_g and decay length λ from the simulations. We have also evaluated the envelope of wave packets from the magnitude of their analytic signal without assumptions of the shape or symmetry of the envelope. The extracted values of the group velocity and decay length using this approach were almost identical to the values obtained from Gaussian fitting, thus giving credence to the fitting approach adopted here.

III. RESULTS AND DISCUSSIONS

Figure 3 shows typical simulated waveforms of various Py film thicknesses for $\sigma_{\text{Py}} = 0$ and 5×10^6 S/m. The distance x from the

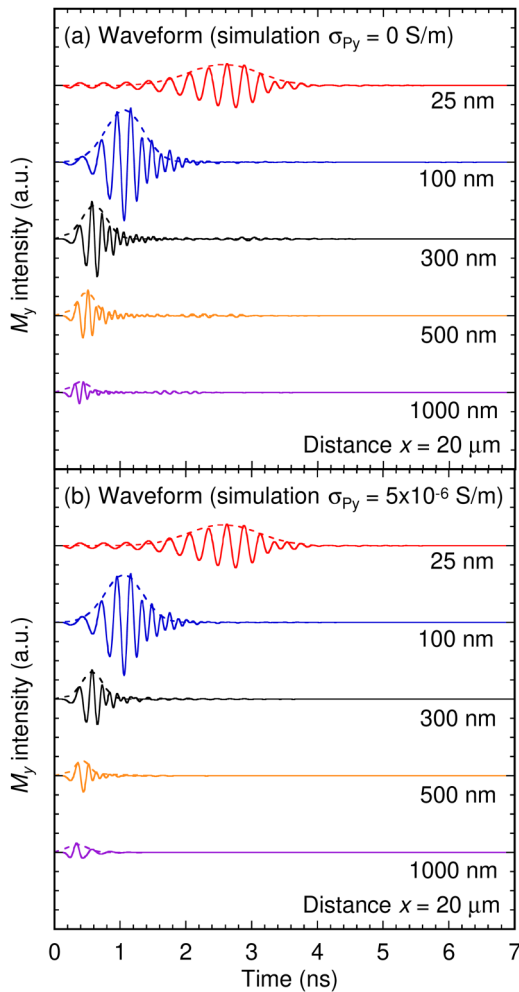


FIG. 3. Typical simulated waveforms of various Py film thicknesses for (a) $\sigma_{\text{Py}} = 0$ S/m and (b) $\sigma_{\text{Py}} = 5 \times 10^6$ S/m. The distance x from the excitation antenna to the detection point is $20 \mu\text{m}$. Dashed lines are Gaussian fitting results of the envelope of the wave packets.

edge of the signal antenna to the detection point is $20 \mu\text{m}$. The dashed lines in the figure are Gaussian fitting results of the envelope of the wave packets. Waveforms for zero and finite Py conductivity are similar for films up to 100 nm thick. For Py thicknesses over 300 nm , however, the waveforms for the conductive films become heavily damped and attenuated. Thus, the conductivity of the waveguide enhances magnetic damping prominently for thick films. The increased damping of the magnetization oscillations in conductive films leads to narrowing of the spin wave envelope with more rapid decay of the upper tail of the wave packet in the direction of increasing time, compared with that of nonconductive films. Consequently, their peak shifts toward shorter times. Therefore, the wave packet arrival time (time at which the waveform envelope is maximum) appears shorter for $\sigma_{\text{Py}} = 5 \times 10^6$ S/m

than for $\sigma_{\text{Py}} = 0$ S/m with increasing Py thickness. The relationship between the distance x along the Py film beyond the edge of the signal conductor and peak arrival time is plotted in Fig. 4. The group velocity v_g can be estimated from the gradient of these straight lines. It can be observed that the gradient of the curves in Fig. 4 and, therefore, v_g increase with increasing thickness of the Py film. Moreover, the gradient of the curves in Fig. 4 for $\sigma_{\text{Py}} = 5 \times 10^6$ S/m becomes steeper than that for $\sigma_{\text{Py}} = 0$ S/m with increasing film thickness and explains the further increase observed in the group velocity in the conductive film. This, as previously described, is attributed to the narrowing of the wave packet distribution and shift of their peaks toward shorter arrival times. This indicates that for thick conductive magnetic films, care must be exercised in evaluating the group velocity from waveform fitting. Evaluation of the group velocity from dispersion relation plots is carried out next and compared to the envelope fitting approach.

Figure 5 is the dispersion relations for Py films of various thicknesses, which were obtained from evaluation of the Fast Fourier Transforms (FFTs) of the simulated magnetization waveforms (averaged through the Py thickness) in both time and space along the Py film.³¹ For $\sigma_{\text{Py}} = 0$ S/m, the gradient of the dispersion

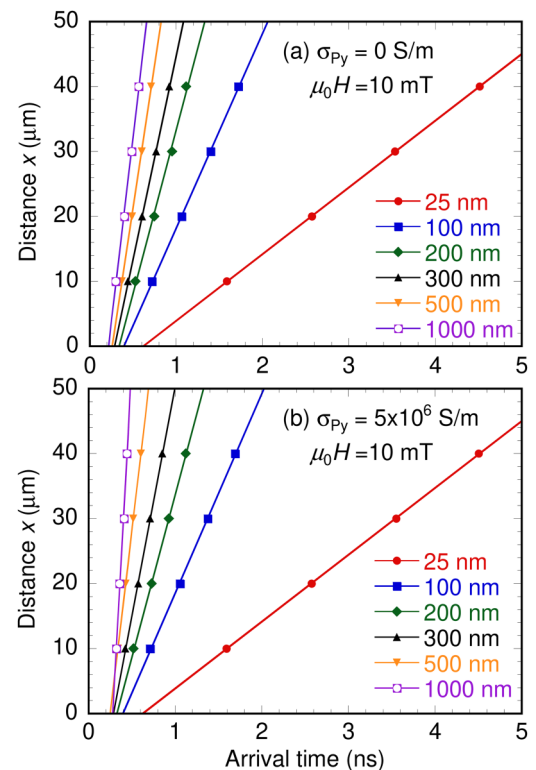


FIG. 4. The relationship between the distance x along the Permalloy film beyond the edge of the signal conductor and peak arrival time (time at which the waveform envelope is maximum): (a) $\sigma_{\text{Py}} = 0$ S/m and (b) $\sigma_{\text{Py}} = 5 \times 10^6$ S/m. The straight lines are obtained by fitting to the magnetization waveforms, and the group velocity v_g values are estimated from the gradient.

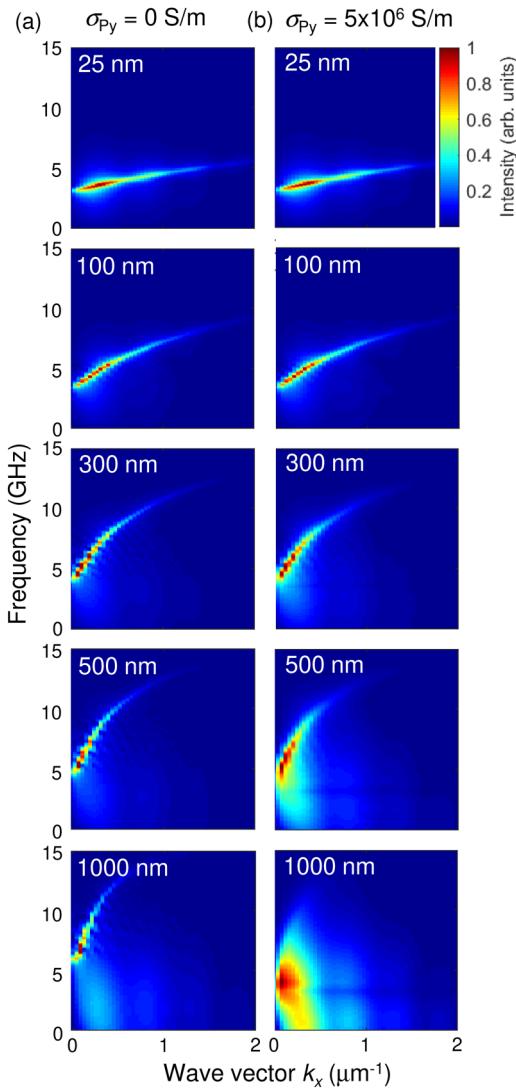


FIG. 5. The dispersion relations of various Py thickness films for (a) $\sigma_{Py} = 0$ S/m and (b) $\sigma_{Py} = 5 \times 10^6$ S/m.

curve and, therefore, v_g increase with increasing Py thickness. For film thicknesses below 100 nm, the dispersion curves for $\sigma_{Py} = 5 \times 10^6$ S/m and $\sigma_{Py} = 0$ S/m are almost identical. The dispersion curves for $\sigma_{Py} = 5 \times 10^6$ S/m, however, become broader for Py films of thicknesses greater than 300 nm, and it is finally indistinctive at a thickness of 1000 nm. It can also be observed from Fig. 5 that the thicker films (500–1000 nm) also exhibit low frequency spectra with increasing intensity. These lower frequency signals originate from forced oscillation near the excitation antenna edge and become more apparent with the decrease in intensity of propagating waves with increasing film thickness. These are localized, stationary oscillations and are not related to propagating MSSW.

Moreover, and for the conductive films in particular, eddy current damping reduces the undamped frequency of the system, which in general may approximately be described by a simple harmonic oscillator: $\omega = \omega_0 \sqrt{1 - \zeta^2}$, where ω_0 is the undamped frequency and ζ is the damping ratio. This leads to the observed increase of the intensity of the low frequency spin wave signals in the simulations for thick conductive films below the Kittel frequency. Thus, normal dispersion curves cannot be clearly obtained in conductive films with large thickness.

The group velocity v_g is now evaluated from the gradient of the dispersion curves in Fig. 5 at $k \sim 0.34 \mu\text{m}^{-1}$. Figure 6 is a summary of the v_g values obtained from the simulations and compared with the experimental measurements from Ref. 24. The v_g values estimated from fitting to the wave packet envelope in Fig. 3 for $\sigma_{Py} = 0$ S/m and $\sigma_{Py} = 5 \times 10^6$ S/m are similar for thicknesses below 100 nm, with increasing difference for thicknesses over 300 nm. The large difference in v_g observed in conductive films for thicknesses over 300 nm in Fig. 6 reflects the shift in the peak time of the magnetization envelope toward shorter times due to increased damping, as seen in Figs. 3 and 4. Thus, conductivity enhances the observed group velocity especially in thick films. The simulated v_g values from fitting to velocity curves in Fig. 4 are in good agreement with the experimental measurements. However, these experimental and simulated results deviate from the calculated v_g values using the analytical formulation.³² The values of v_g calculated from the gradient of the dispersion curves in Fig. 5 at $k \sim 0.34 \mu\text{m}^{-1}$ are also plotted in Fig. 6, and these are in excellent agreement with the analytical solution for both $\sigma_{Py} = 0$ S/m and $\sigma_{Py} = 5 \times 10^6$ S/m. These results indicate that there is no difference in the dispersion relation at the fundamental wavenumber regardless of the conductivity of the Py film.

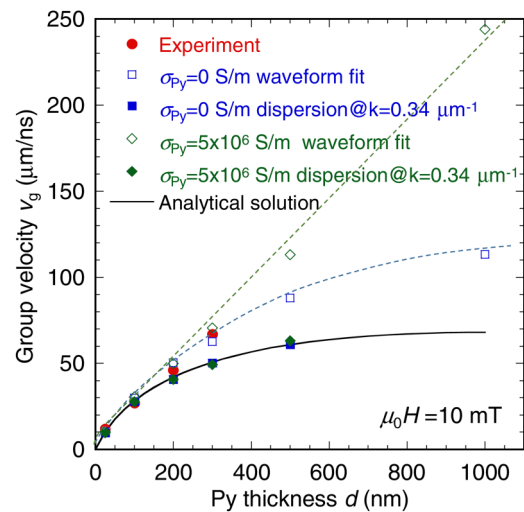


FIG. 6. Summary of the group velocity v_g values as a function of film thickness. Red circles are experimental results and the black solid line is the analytical solution. Blue and green marks are simulation results for $\sigma_{Py} = 0$ S/m and $\sigma_{Py} = 5 \times 10^6$ S/m, respectively. The dashed lines are used for guidance and to illustrate trends.

The difference between the group velocity obtained from fitting to the spin wave envelope in measurements and simulations and the group velocity from the analytical theory at the fundamental wavenumber is due to the dispersive nature of the waves excited by the antenna field. In Fig. 5, the red color in the dispersion curve indicates the largest intensity in the spin wave spectrum. For a 25 nm-thick film, the wavenumber k_x showing the strongest intensity is about $0.34 \mu\text{m}^{-1}$, which is in good agreement with the value estimated from the antenna configuration. The strong intensity region, however, shifts to lower k_x values with increasing Py thickness. For lower k_x values, since the gradient of the dispersion curve increases, v_g should also increase. Thus, the v_g values estimated at the wavenumbers that give the largest spin wave intensity are in good agreement with the results obtained from the waveform fitting for both $\sigma_{\text{Py}} = 0 \text{ S/m}$ and $\sigma_{\text{Py}} = 5 \times 10^6 \text{ S/m}$ (not shown). Therefore, it is inappropriate to estimate v_g from the dispersion relation at the same k_x for thick films due to the shift in the maximum intensity of the dispersion plot to lower wavenumbers. Thus, antenna-excited spin waves are dispersive since they contain many k_x vectors, and the dominant k_x is not determined only by the antenna configuration in thicker films. This is the origin of the deviation of v_g values between estimations from the waveform fitting and those estimated from the analytical formulation. This finding is important to design future spin wave devices.

Figure 7 shows the variation of the amplitude of the simulated spin waves with distance from the edge of the signal conductor ($x=0$). The amplitude variation clearly shows exponential decay with increasing distance x . The decay length λ is estimated by exponential fitting and summarized in Fig. 8 for different Py film thicknesses. The decay length λ increases monotonically for $\sigma_{\text{Py}} = 0 \text{ S/m}$, as expected from the increase of v_g . For $\sigma_{\text{Py}} = 5 \times 10^6 \text{ S/m}$, on the other hand, λ initially increases with increasing thickness but then begins to decrease for thicker films. This behavior of the simulation results for $5 \times 10^6 \text{ S/m}$ agrees well with the experimental results and again confirms the validity of the numerical model and waveform fitting approach to extract wave packet amplitude information. The simulated difference in the decay length of the spin waves between the nonconductive and conductive films is only 5.6% for the 100 nm film and increases to 15% for the 200 nm film. Thus, the electrical conductivity of the Py film enhances the attenuation of the spin wave propagation and indicates that the influence of the conductivity on spin wave propagation cannot be ignored for metal films thicker than 200 nm. These results suggest that the metal thickness of a waveguide should be less than 100 nm.

The decay length can be described as a function of the damping factor α using²⁰

$$\lambda = \frac{\left(\frac{M_S}{2}\right)^2 t \exp(-2kd)}{\alpha(\mu_0 H + \frac{M_S}{2}) \sqrt{\mu_0 H(\mu_0 H + M_S) + \left(\frac{M_S}{2}\right)^2 (1 - \exp(-2kd))}}, \quad (6)$$

where α is independent of k and the bias magnetic field, and so the damping mechanism does not depend on the antenna configuration and bias field. Using the calculated decay lengths of the spin

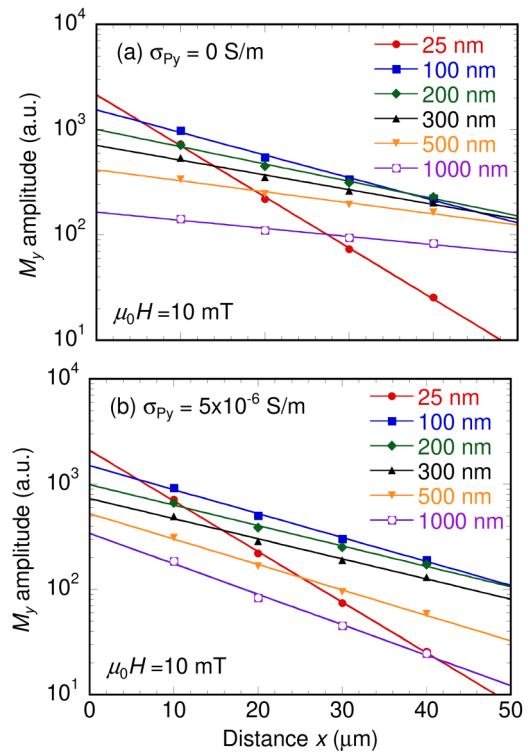


FIG. 7. The variation of the amplitude of the simulated y-component of the magnetization with distance from the edge of the signal conductor for (a) $\sigma_{\text{Py}} = 0 \text{ S/m}$ and (b) $\sigma_{\text{Py}} = 5 \times 10^6 \text{ S/m}$. The straight lines are obtained by fitting, and the decay lengths λ are estimated from the gradient.

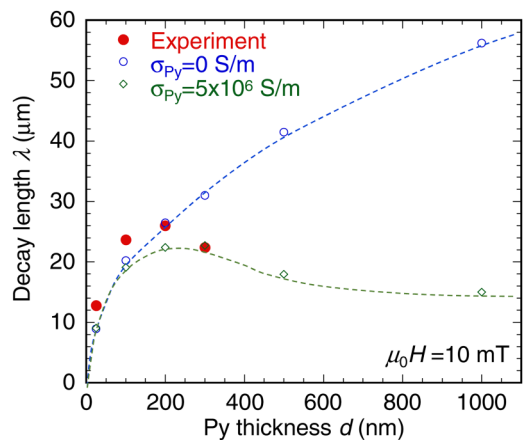


FIG. 8. Summary of the decay length λ variation with film thickness. Red circles are experimental results. Blue and green marks are simulation results for $\sigma_{\text{Py}} = 0 \text{ S/m}$ and $\sigma_{\text{Py}} = 5 \times 10^6 \text{ S/m}$, respectively. The dashed lines are used for guidance and to illustrate trends.

wave amplitudes from Fig. 8, the damping factor was estimated as a function of film thickness. The values of the wavenumber k_x used to estimate the damping factor are the values that give the largest spin wave intensity in the simulated spectra for each Py thickness. The α values extracted from the experiments and simulations are summarized in Fig. 9. The error bars were calculated assuming that k_x is shifted by $\pm 0.05 \mu\text{m}^{-1}$, which roughly corresponds to the FFT resolution due to limitation of the simulated system size, and the deviation becomes large with thickness. As seen in Fig. 9, α increases with increasing Py thickness, and the results of the simulation and experiment agree well. In this case, α consists of the intrinsic contribution of damped precession α_0 and eddy current contribution α_{eddy} . The damping due to eddy currents α_{eddy} for a thin film can be expressed as³³

$$\alpha_{\text{eddy}} = P\mu_0 M_S \gamma \sigma d^2, \quad (7)$$

where μ_0 is the vacuum permeability, t is the metal thickness, and P is a configuration-dependent coefficient. In the case of uniaxial magnetocrystalline anisotropy and bias field both perpendicular to the film plane, P increases from 0 at the surface to a value of 1/8 at the film center.³³ In Ref. 23, P is written as 1/6, but there is no derivation and the magnetic field direction is not specified, and so an applicable range is ambiguous. In addition to the thin film structure, α_{eddy} values for a sphere, a cube, and a prism were also derived³⁴ and indicated in the case of prisms the anisotropic nature of α_{eddy} . P for MSSW is, however, still unknown. The solid and dashed lines in Fig. 9 are the calculated curves of $\alpha = \alpha_0 + \alpha_{\text{eddy}}$ for $\alpha_0 = 0.01$ and $P = 1/4$ (solid) and $1/3$ (dashed). Compared to the experimental and simulated results, the eddy current damping seems to be proportional to d^2 as expressed in Eq. (7). The coefficient P is likely to be between 1/3 and 1/4 for MSSW propagation

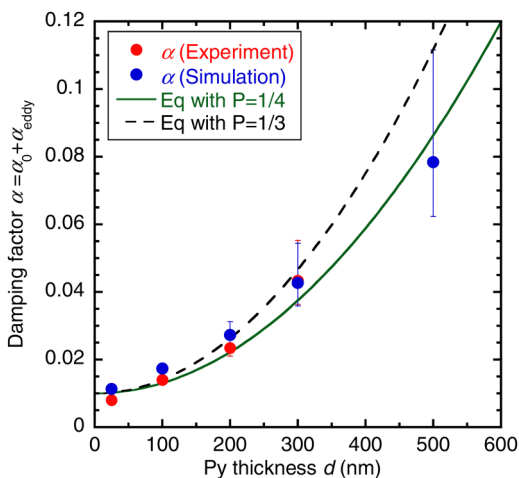


FIG. 9. Damping factor α from experiments and simulations estimated from the decay length. The error bars were calculated assuming that k is shifted by $\pm 0.05 \mu\text{m}^{-1}$. The solid and dashed lines are the calculated curves of $\alpha = \alpha_0 + \alpha_{\text{eddy}}$ for $\alpha_0 = 0.01$ and $C = 1/4$ (solid) and $1/3$ (dashed) using Eq. (6).

based on the comparison with the experimental and simulation results in Fig. 9. Furthermore, Ref. 34 indicated the anisotropic nature of α_{eddy} in prisms based on the direction of magnetization change, geometry, and excitation field direction and, hence, the likely variation of P with film thickness. Thus, the thickness dependence of α also supports the nonmonotonous behavior of the decay length change with thickness originating from the eddy currents in conductive films.

IV. CONCLUSION

The influence of the conductivity of a Permalloy waveguide on the spin wave propagation was investigated using finite-element simulations of the quasistatic electromagnetic fields and the linearized LLG equation. The group velocity v_g estimated from fitting to the simulated dynamic magnetization waveforms showed good agreement with the experimental results. The difference in v_g between $\sigma_{\text{Py}} = 0 \text{ S/m}$ and $\sigma_{\text{Py}} = 5 \times 10^6 \text{ S/m}$ becomes large for film thicknesses over 300 nm, though the difference is very small for film thicknesses less than 100 nm. This enhancement of v_g originates from the damping due to the conductivity of the films, causing narrowing of the spin wave envelope and shift of its peak toward shorter arrival times with increasing thickness. The basic characteristics of the dispersion relations do not change between the conductive and nonconductive films for thicknesses below 300 nm. For conductive films, however, the dispersion relation becomes broader with increasing thickness and is finally indistinctive for a 1000 nm-thick film. The dispersive spin waves excited by the antenna cause the deviation of v_g values from the simulations and experimental measurements from the analytical formulation for the insulating material. For thick films, the dominant wavenumber of the excited spin wave shifts from the wavenumber estimated by the antenna configuration toward lower wavenumbers. Therefore, using the same wavenumber in the estimation of v_g from the dispersion relation in films of different thicknesses leads to incorrect values because of the change in the fundamental wavenumber with thickness. The decay length λ for conductive films was found to initially increase with thickness but then decrease for increasing thicknesses beyond 200 nm. This nonmonotonous behavior found from simulations is in good agreement with the experimental results over the same film thickness range. The nonmonotonous dependence of the decay length on thickness is due to the additional damping due to the electrical conductivity of the film. As a result, the damping coefficient α extracted from both simulations and experimental measurements increases proportionally with d^2 , where d is the film thickness and, hence, is significantly enhanced for thick films. Thus, the conductivity influences the apparent group velocity and decay length particularly in thick films. These results suggest that the metal thickness of a waveguide should be less than 100 nm for future spin wave device applications.

ACKNOWLEDGMENTS

T.M. would like to thank Professor V. V. Kruglyak for fruitful discussions. This work was partly supported by the JSPS KAKENHI (Grant Nos. 24560034 and 15K06000). This work was supported in part by funds (Nos. 167003 and 175005) from the Central Research Institute of Fukuoka University.

REFERENCES

- ¹V. V. Kruglyak, S. O. Demokritov, and D. Grundler, *J. Phys. D* **43**, 264001 (2010).
- ²A. Khitun, M. Bao, and K. L. Wang, *J. Phys. D* **43**, 264005 (2010).
- ³B. Lenk, H. Ulrichs, F. Garbs, and M. Münzenberg, *Phys. Rep.* **507**, 107 (2011).
- ⁴Y. Au, M. Dvornik, O. Dmytriiev, and V. V. Kruglyak, *Appl. Phys. Lett.* **100**, 172408 (2012).
- ⁵A. Khitun, *J. Appl. Phys.* **111**, 054307 (2012).
- ⁶A. V. Chumak, A. A. Serga, and B. Hillebrands, *Nat. Commun.* **5**, 4700 (2014).
- ⁷K. Vogt, F. Y. Fradin, J. E. Pearson, T. Sebastian, S. D. Badar, B. Hillebrands, A. Hoffmann, and H. Schultheiss, *Nat. Commun.* **5**, 3727 (2014).
- ⁸M. Vogel, A. V. Chumak, E. H. Waller, T. Langner, V. I. Vasyuchka, B. Hillebrands, and G. von Freymann, *Nat. Phys.* **11**, 487 (2015).
- ⁹A. V. Chumak, V. I. Vasyuchka, A. A. Serga, and B. Hillebrands, *Nat. Phys.* **11**, 453 (2015).
- ¹⁰N. Kanazawa, T. Goto, K. Sekiguchi, A. B. Granovsky, C. A. Ross, H. Takagi, Y. Nakamura, and M. Inoue, *Sci. Rep.* **6**, 30268 (2016).
- ¹¹A. Haldar, D. Kumar, and A. O. Adeyeye, *Nat. Nanotech.* **11**, 437 (2016).
- ¹²L. J. Cornelissen, J. Liu, B. J. V. Wees, and R. A. Duine, *Phys. Rev. Lett.* **120**, 097702 (2018).
- ¹³M. Bailleul, D. Olligs, C. Fermon, and S. O. Demokritov, *Europhys. Lett.* **56**, 741 (2001).
- ¹⁴M. Covington, T. M. Crawford, and G. J. Parker, *Phys. Rev. Lett.* **89**, 237202 (2002).
- ¹⁵V. Vlaminck and M. Bailleul, *Science* **322**, 410 (2008).
- ¹⁶M. Zhu, C. L. Dennis, and R. D. McMichael, *Phys. Rev. B* **81**, 140407(R) (2010).
- ¹⁷K. Sekiguchi, K. Yamada, S.-M. Seo, K.-J. Lee, D. Chiba, K. Kobayashi, and T. Ono, *Phys. Rev. Lett.* **108**, 017203 (2012).
- ¹⁸K. Yamanoi, S. Yakata, T. Kimura, and T. Manago, *Jpn. J. Appl. Phys.* **52**, 083001 (2013).
- ¹⁹N. Sato, K. Sekiguchi, and Y. Nozaki, *Appl. Phys. Exp.* **6**, 063001 (2013).
- ²⁰T. Manago, K. Yamani, S. Kasai, and S. Mitani, *J. Appl. Phys.* **117**, 17D121 (2015).
- ²¹K. Kasahara, M. Nakayama, X. Ya, K. Matsuyama, and T. Manago, *Jpn. J. Appl. Phys.* **56**, 010309 (2017).
- ²²K. Shibata, K. Kasahara, K. Nakayama, V. V. Kruglyak, M. M. Aziz, and T. Manago, *J. Appl. Phys.* **124**, 243901 (2018).
- ²³A. Barman and S. Sinha, *Spin Dynamics and Damping in Ferromagnetic Thin Film and Nanostructures* (Springer, 2018), p. 30.
- ²⁴M. Ota, K. Yamanoi, S. Kasai, S. Mitani, and T. Manago, *Jpn. J. Appl. Phys.* **54**, 113001 (2015).
- ²⁵W. S. Ament and G. T. Rado, *Phys. Rev.* **97**, 1558 (1955).
- ²⁶N. S. Almeida and D. L. Mills, *Phys. Rev. B* **53**, 12232 (1996).
- ²⁷I. S. Maksymov and M. Kostylev, *J. Phys. D Appl. Phys.* **46**, 495001 (2013).
- ²⁸T. L. Gilbert, *IEEE Trans. Magn.* **40**, 3443 (2004).
- ²⁹A. F. Mayadas, J. F. Janak, and A. Gangulee, *J. Appl. Phys.* **45**, 2780 (1974).
- ³⁰V. Vlaminck and M. Bailleul, *Phys. Rev. B* **81**, 014425 (2010).
- ³¹M. Dvornik, Y. Au, and V. V. Kruglyak, in *Magnonics*, Topics in Applied Physics Vol. 125, edited by S. Demokritov and A. Slavin (Springer, 2013), p. 101.
- ³²D. D. Stancil and A. Prabhakar, *Spin Waves—Theory and Applications* (Springer, 2009), p. 163.
- ³³A. Magni, G. Bertotti, I. D. Mayergoyz, and C. Serpico, *Physica B* **306**, 121 (2001).
- ³⁴E. Martinez, L. Lopez-Diaz, and L. Torres, *J. Appl. Phys.* **99**, 123912 (2006).